nature chemistry

ARTICLES

PUBLISHED ONLINE: 19 DECEMBER 2016 | DOI: 10.1038/NCHEM.2686

Atomically precise organomimetic cluster nanomolecules assembled via perfluoroaryl-thiol S_NAr chemistry

Elaine A. Qian[1,2,3], Alex I. Wixtrom[1], Jonathan C. Axtell[1], Azin Saebi[1], Dahee Jung[1,3], Pavel Rehak[4], Yanxiao Han[4], Elamar Hakim Moully[1], Daniel Mosallaei[1], Sylvia Chow[1], Marco S. Messina[1,3], Jing Yang Wang[1], A. Timothy Royappa[5], Arnold L. Rheingold[6], Heather D. Maynard[1,3], Petr Král[4,7,8] and Alexander M. Spokoyny[1,3]*

The majority of biomolecules are intrinsically atomically precise, an important characteristic that enables rational engineering of their recognition and binding properties. However, imparting a similar precision to hybrid nanoparticles has been challenging because of the inherent limitations of existing chemical methods and building blocks. Here we report a new approach to form atomically precise and highly tunable hybrid nanomolecules with well-defined three-dimensionality. Perfunctionalization of atomically precise clusters with pentafluoroaryl-terminated linkers produces size-tunable rigid cluster nanomolecules. These species are amenable to facile modification with a variety of thiol-containing molecules and macromolecules. Assembly proceeds at room temperature within hours under mild conditions, and the resulting nanomolecules exhibit high stabilities because of their full covalency. We further demonstrate how these nanomolecules grafted with saccharides can exhibit dramatically improved binding affinity towards a protein. Ultimately, the developed strategy allows the rapid generation of precise molecular assemblies to investigate multivalent interactions.

Natural systems feature very complex three-dimensional (3D) molecular architectures that can interact with a high degree of specificity and fidelity. Among the well-established interaction modes, multivalency has been known to enable myriad biological events by strengthening individually weak interactions between biomolecules that are either native or foreign to the organism[1]. Multivalent interactions can be found in such diverse processes as infection (viral/bacterial proteins–cell receptors), immune recognition (antibodies–cell receptors/antigens, cytokines–cell receptors) and gene-expression regulation (transcription factors–DNA) because of the higher avidity and better recognition compared with the corresponding monovalent bindings[1,2].

Inspired by nature's design, chemists have taken an interest in developing synthetic multivalent ligands with the ability to bind specific target receptors with a high affinity to (1) elucidate the mechanistic details of multivalent interactions and (2) promote or inhibit biological interactions of interest[3]. Many examples of synthetic scaffolds have emerged over the past several decades[4–18], which include, but are not limited to, polymeric nanoparticles[4,5], dendrimers[6,7] and hybrid nanoparticles[8–16]. Specifically, the advent of nanotechnology and the development of surface-functionalized metal nanoparticles has provided an extremely powerful class of multivalent scaffolds. For example, gold nanoparticles (AuNPs) capped with thiolated ligands can feature biocompatibility and stability, which enables them for applications that require binding and recognition capabilities[10,11]. Hybrid AuNP systems are especially attractive because of the synthetic ease of producing systems that are well-defined and tunable in size. Nevertheless, it is well known that thiolated ligands often can desorb or undergo exchange processes with other surfactants in solution over short periods of time, and furthermore, various electrochemical conditions or elevated temperatures (>60 °C) dramatically accelerate these processes[10,19–22]. These events can be explained primarily by the relatively weak nature of the gold–thiolate bond (40–50 kcal mol^{-1}) (ref. 19). Processes of thiol-ligand exchange also readily occur on smaller Au-based cluster molecules (≤5 nm), which potentially limits the ability of researchers to create atomically precise hybrid nanomolecules that remain compositionally well-defined under biologically relevant conditions (for example, in serum)[21,23].

Here we report a new strategy to build robust atomically precise hybrid nanomolecules using air-stable inorganic clusters[24–30] densely decorated with perfluoroaromatic functional groups. Using this organomimetic strategy[29], we show that one can mimic the rigid surface of a Au-based nanoparticle core and simultaneously produce assemblies that are fully covalent and thus stable under relatively harsh conditions (Fig. 1). Specifically, we demonstrate how dodecaborate clusters[29,31–36] that feature a dense layer of rigid pentafluoroaryl functional groups can serve as excellent scaffolds for constructing atomically precise multivalent organomimetic cluster nanomolecules (OCNs). The perfluoroaryls are able to undergo facile 'click'-like nucleophilic aromatic substitution (S_NAr) with a wide range of thiols at room temperature within hours, which

[1]Department of Chemistry and Biochemistry, University of California, Los Angeles, California 90095, USA. [2]Department of Bioengineering, University of California, Los Angeles, California 90095, USA. [3]California NanoSystems Institute, University of California, Los Angeles, California 90095, USA. [4]Department of Chemistry, University of Illinois at Chicago, Chicago, Illinois 60607, USA. [5]Department of Chemistry, University of West Florida, Pensacola, Florida 32514, USA. [6]Department of Chemistry and Biochemistry, University of California, San Diego, La Jolla, California 92093, USA. [7]Department of Physics, University of Illinois at Chicago, Chicago, Illinois 60607, USA. [8]Department of Biopharmaceutical Sciences, University of Illinois at Chicago, Chicago, Illinois 60612, USA. *e-mail: spokoyny@chem.ucla.edu

© 2017 Macmillan Publishers Limited, part of Springer Nature. All rights reserved.

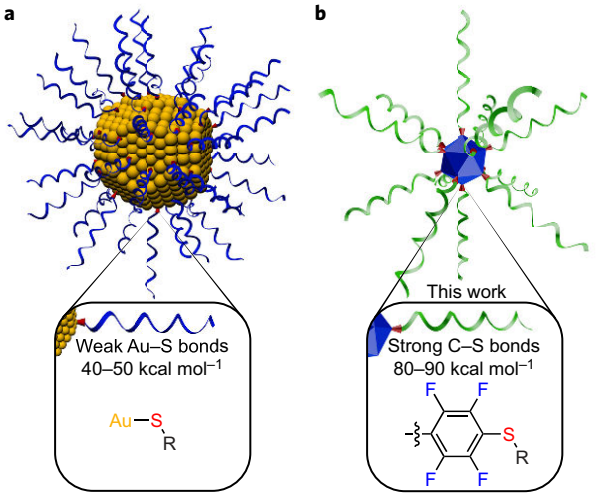


Figure 1 | Comparison of features between the thiol-capped AuNPs and the OCNs. a, Thiol-capped AuNPs between 5 and 100 nm can be easily prepared via self-assembly to give rise to polydisperse hybrid particles that comprise weak, non-covalent gold–thiolate bonds (40–50 kcal mol^{-1}). These AuNPs often undergo ligand-exchange processes that can compromise the structural integrity of the particles. **b**, Uniform and robust OCNs can be assembled efficiently with atomic precision and full covalency in the size range 2–10 nm via perfluoroaryl-thiol S_NAr chemistry under mild conditions. The formed carbon–sulfur bond (80–90 kcal mol^{-1}) is significantly stronger compared with the gold–sulfur interaction, and results in nanomolecules that feature high structural stabilities.

creates robust carbon–sulfur bonds (80–90 kcal mol^{-1}) (ref. 37) and thereby produces nanomolecules decorated with well-defined functional surfaces. This approach affords the functional advantages of using dendrimers and at the same time mimicking the synthetic ease with which thiol-capped AuNPs are normally constructed. Unlike the majority of dendritic scaffolds[38,39], the resulting assemblies are highly rigid and can be synthesized and purified within hours. Furthermore, these OCNs are purely covalent and therefore feature improved stability in serum and various pH environments. Finally, we demonstrate the first example of using a hybrid inorganic cluster scaffold as a highly competent multivalent recognition platform for binding a protein system.

Results and discussion

Given the high reactivity of the perfluoroarenes with thiol-based nucleophiles[40–44], we hypothesized that perfluoroaryl-thiol S_NAr chemistry could be utilized to conjugate various thiolated groups onto perfluoroaryl-containing clusters efficiently under mild conditions at room temperature. Recently, our laboratory reported a rapid perfunctionalization strategy of the $[B_{12}(OH)_{12}]^{2-}$ cluster (**1**), originally discovered by Hawthorne and co-workers[31–34], that features a wide scope of substituents[35]. Using this method, we synthesized perfunctionalized clusters grafted with rigid linkers that contained peripheral pentafluoroaryl moieties (Fig. 2a). Specifically, the perfunctionalized cluster scaffolds **2** and **3** can be synthesized in good yields in less than 30 minutes and isolated after purification by silica-gel column chromatography in their neutral form as air-stable solids soluble in the majority of common polar organic solvents (Supplementary pages 9–12). The single-crystal X-ray structures of **2** and **3** reveal the highly rigid nature of these scaffolds (Fig. 2b,c, respectively). Importantly, by using a size-tunable linker precursor in the synthesis of **2** and **3**, the resulting rigid cluster species can be rationally controlled in size (**2** is approximately 1.9 and **3** is about 2.7 nm lengthwise, as measured from the single-crystal structures). These clusters represent a new class of atomically precise scaffolds that offer unique rigidity and structural covalency, which makes them topologically reminiscent of both dendrimers and small metal nanoparticles.

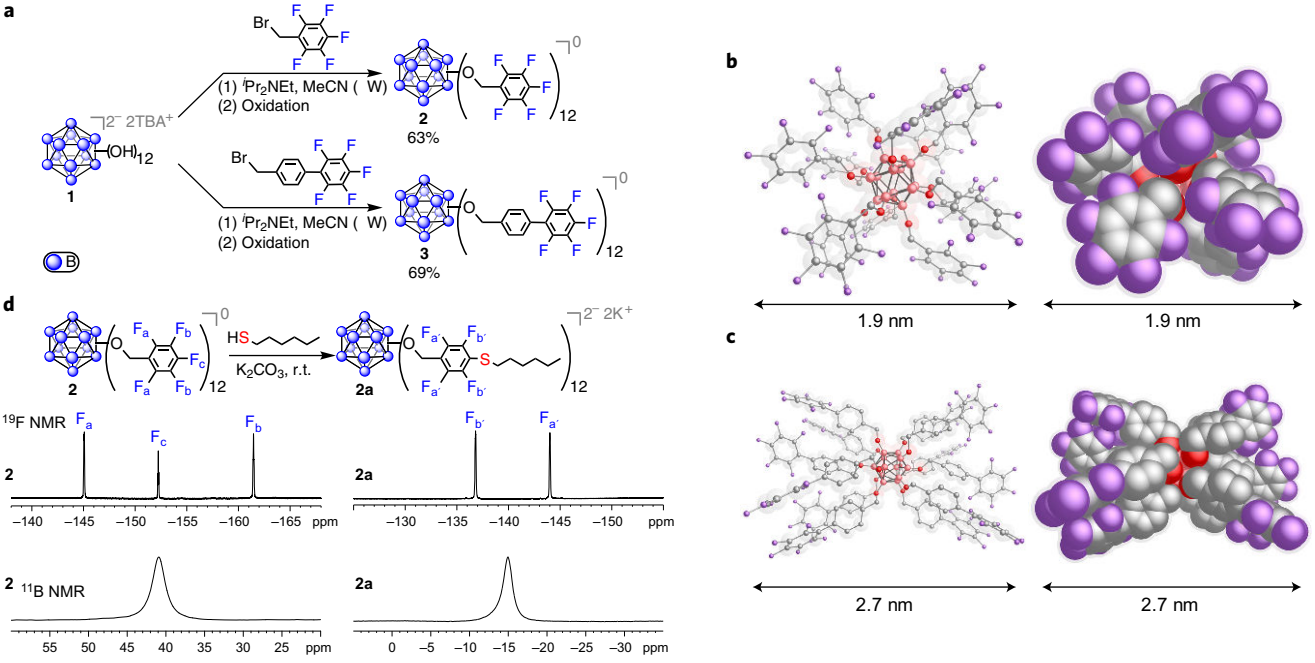
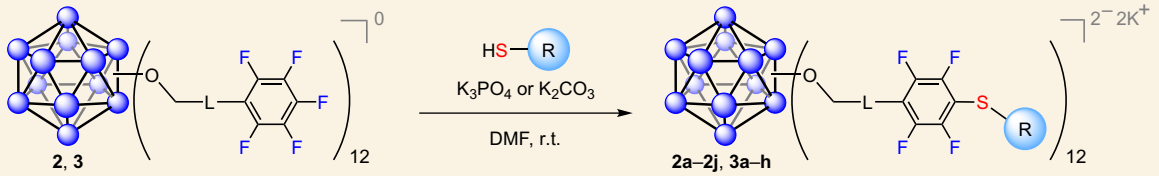
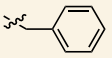
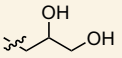
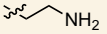
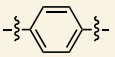
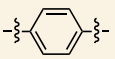
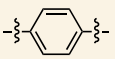
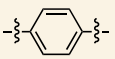
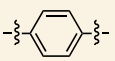
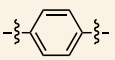
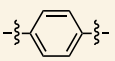
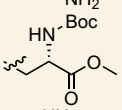
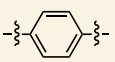
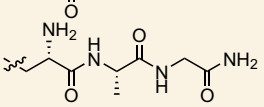


Figure 2 | Synthesis and characterization of the perfluoroaryl-perfunctionalized dodecaborate clusters and the subsequent modification with thiols. **a**, Perfunctionalization of **1** with rigid pentafluoroaryl-terminated linkers yields pure clusters **2** and **3**, after isolation. **b**,**c**, Ball-and-stick and space-filling representations of the single-crystal X-ray structures of **2** and **3**, respectively. Size measurements of the crystal structures reveal that **2** is 1.9 nm and **3** is 2.7 nm (lengthwise). B, pink; O, red; C, grey; F, purple. **d**, 'Click'-like modification of cluster **2** with the 1-hexanethiol reagent and the corresponding ^{19}F and ^{11}B NMR spectra associated with the transformation from the starting material **2** to the functionalized product **2a**. Specifically, perfunctionalization of **2** with 1-hexanethiol results in a shift of the *meta*-F resonance and the complete disappearance of the *para*-F resonance as well as a characteristic upfield shift of the boron singlet that results from the reduction of the cluster. TBA, tetrabutylammonium.

© 2017 Macmillan Publishers Limited, part of Springer Nature. All rights reserved.

Table 1 | Conjugation Scope for 2 and 3.



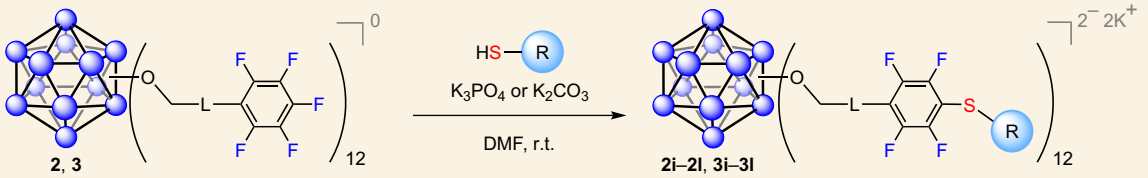
Entry	Compound	L	R	Time (h)	*In situ* yield* (%)	Isolated yield† (%)
1	**2a**	None		24	99	70
2	**2b**	None		24	99	90
3	**2c**	None		24	99	94
4	**2d**	None		24	99	40
5	**2e**	None		24	99	30
6	**2f**	None		24	99	49
7	**3a**			7‡	99	87
8	**3b**			7‡	99	85
9	**3c**			5	99	81
10	**3d**			2	99	81
11	**3e**			4	99	59
12	**3f**			3	99	33
13	**3g**			3	99	49
14	**3h**§			6	99	29

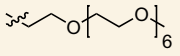
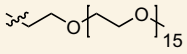
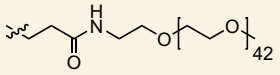
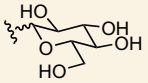
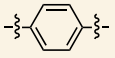
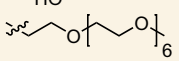
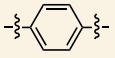
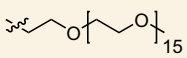
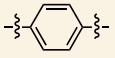
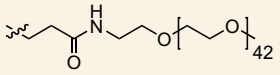
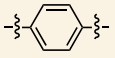
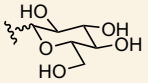
*Yield determined by ^{19}F NMR spectroscopy; †Isolated yields after purification; ‡Small-scale reactions show full conversion within 1 h; §Additional 36 equiv. isopropoxytrimethylsilane (^{i}PrMe$_3$Si) was employed to scavenge fluoride (F^-) by-product. r.t., room temperature.

To test our hypothesis that **2** and **3** could be fully functionalized by thiols via an S_NAr reaction, we commenced conjugation studies between **2** and 1-hexanethiol (**A**). Cluster **2** was mixed with 12 equiv. of thiol **A** in dimethylformamide (DMF) in the presence of base and left stirring under a N_2 atmosphere to mitigate the undesired oxidation of the thiol reagent. Notably, the initially dark-red solution quickly turned colourless. ^{11}B NMR spectroscopy of this colourless solution revealed a singlet resonance at $\delta = 15$, characteristic of a reduced cluster in a $[\mathbf{2}]^{2-}$ oxidation state[35,36], which is consistent with the reducing capacity of the thiolate species when exposed to $[\mathbf{2}]^0$ (Fig. 2d). Therefore, for all subsequent optimization studies we utilized an extra equivalent of the thiol reagent to account for this reduction (Supplementary Table 1). ^{19}F NMR spectroscopy was utilized to monitor the conversion of **2** into **2a**, given the diagnostic change associated with this transformation (Fig. 2d shows the disappearance of the *para*-F resonance and significant downfield shift of the *meta*-F resonances in **2a** compared with the that of starting material **2**). A base screen identified potassium carbonate (K_2CO_3) as the optimal reagent that leads to the substantial conversion that resulted in the formation of the perfunctionalized cluster **2a** (Supplementary Table 1, entry 4). After additional optimization using K_2CO_3, we found that using 13.3 equiv. of 1-hexanethiol and 30 equiv. of K_2CO_3 resulted in a nearly quantitative (>99%) substitution of **2**, to produce the 12-fold substituted OCN **2a** (Fig. 2d and Table 1, entry 1). The crude product was dried and then purified via silica gel column chromatography and isolated as an oily substance in 70% yield (Supplementary pages 13 and 14). Electrospray ionization-high resolution mass spectrometry (ESI-HRMS) and ^{1}H, ^{11}B and ^{19}F NMR spectroscopies of purified **2a** are consistent with its proposed structure and composition (Supplementary pages 51–55). Further, we found that **2** could be conjugated fully with aromatic (**B**) and benzylic (**C**) thiols. Both reactions proceeded nearly quantitatively within 24 hours at room temperature using potassium phosphate (K_3PO_4), and led to pure OCNs **2b** and **2c** (Table 1,

© 2017 Macmillan Publishers Limited, part of Springer Nature. All rights reserved.

Table 2 | PEGylation and glycosylation of 2 and 3.



Entry	Compound	L	R	Time (h)	*In situ* yield* (%)	Isolated yield† (%)
1	**2i**	None		24	99	81
2	**2j**	None		24	99	19
3	**2k**	None		24	99	41
4	**2l**‡	None		24	99	17
5	**3i**			5	99	78
6	**3j**			4	99	21
7	**3k**			20§	99	54
8	**3l**‡			5	99	32

*Yield determined by ^{19}F NMR spectroscopy; †Isolated yields after purification; ‡2l and 3l underwent partial K^+/Na^+ counterion exchange during the deprotection reaction with NaOMe; §Small-scale reaction shows full conversion within 5 h.

entries 2 and 3), respectively, after isolation in good yields (Supplementary pages 14–16 and 56–69 give details on the reaction conditions, purification and characterization). Importantly, the results with 2a–2c indicate that the developed chemistry can operate with a wide range of thiol-based species that span a significant window of nucleophilicities (the pK_a of aliphatic thiols is approximately 17, and that of aromatic thiols is approximately 10). Overall, these experiments suggest that, with the developed method, it is possible to assemble OCNs rapidly via S_NAr chemistry under very mild and operationally simple conditions that mimic the simplicity of the assembly of thiol-capped AuNPs. Furthermore, unlike the previously developed Huisgen 'click' cycloaddition and carbamate functionalization strategies of inherently non-rigid B_{12}-based clusters, which require elevated temperatures, long reaction times (days) and a large excess of reagents (4–5-fold per vertex), the perfluoroaryl-thiol S_NAr chemistry described here proceeds using significantly milder conditions[33,34].

Thiol-capped AuNP constructs are also extremely attractive given the chemical orthogonality of the gold–thiol interaction compared with that of other ligands, which provides an opportunity to use a wide variety of unprotected thiol reagents for facile and programmable self-assembly. Therefore, we decided to probe the degree to which S_NAr chemistry on perfluorinated clusters can mimic this attractive feature. To evaluate the thiol selectivity of our approach, we performed conjugation reactions between **2** and thiols that featured additional nucleophilic groups, such as alcohols and amines. Consistent with the previous work by Pentelute and co-workers with unprotected peptides[43,44], we found that the model thiol species (**D**–**F**) all reacted with **2** through the thiol site selectively to form the desired perfunctionalized OCNs 2d–2f (Table 1, entries 4–6) within 24 hours, as confirmed by ^{19}F NMR spectroscopy (Supplementary pages 16–19 and 139–159 give details on the reaction conditions, purification and characterization). This finding is important as it suggests that this chemistry can be used to conjugate selectively thiol reagents that contain multiple nucleophilic functional groups and fundamentally takes advantage of the mild conditions developed here, which allow one to guide the kinetic selectivity between the thiol and pentafluoroaryl fragment[42–44]. Most importantly, this chemoselectivity is reminiscent of that observed in the assembly of thiol-capped AuNPs.

With the successful perfunctionalization of **2** (*vide supra*), we hypothesized that the larger-sized cluster **3** could not only be perfunctionalized with the same thiols to create a new generation of OCNs that are modularly extended in size, but could also accommodate 12-fold conjugation with bulkier substrates. Indeed, under the same conditions as described above for the functionalization of **2**, cluster **3** undergoes clean and facile perfunctionalization chemistry with thiols **A**–**F** to yield 3a–3f (Table 1, entries 7–12 and Supplementary pages 25–31 and 118–159). Importantly, when using **3** instead of **2**, we observed a significantly faster conversion rate that led to perfunctionalized clusters (less than six hours versus 24 hours), consistent with the surface of **3** being less sterically encumbered than that of **2**. Therefore, using **3** allowed full substitution with a bulky cysteine derivative (**G**) as well as a small, unprotected peptide sequence C-A-G (**H**) to yield 3g and 3h, respectively (Table 1, entries 13 and 14 and Supplementary pages 31–33, 160–173 and 222).

Next, to test whether more-complex molecular architectures could also be introduced onto the clusters, we turned our attention to poly(ethylene glycol) (PEG)[4,22,45,46]. Complete 12-fold conjugation between **2** and commercially available mPEG-thiol (M_w = 356 Da) occurred within 24 hours at room temperature to

© 2017 Macmillan Publishers Limited, part of Springer Nature. All rights reserved.

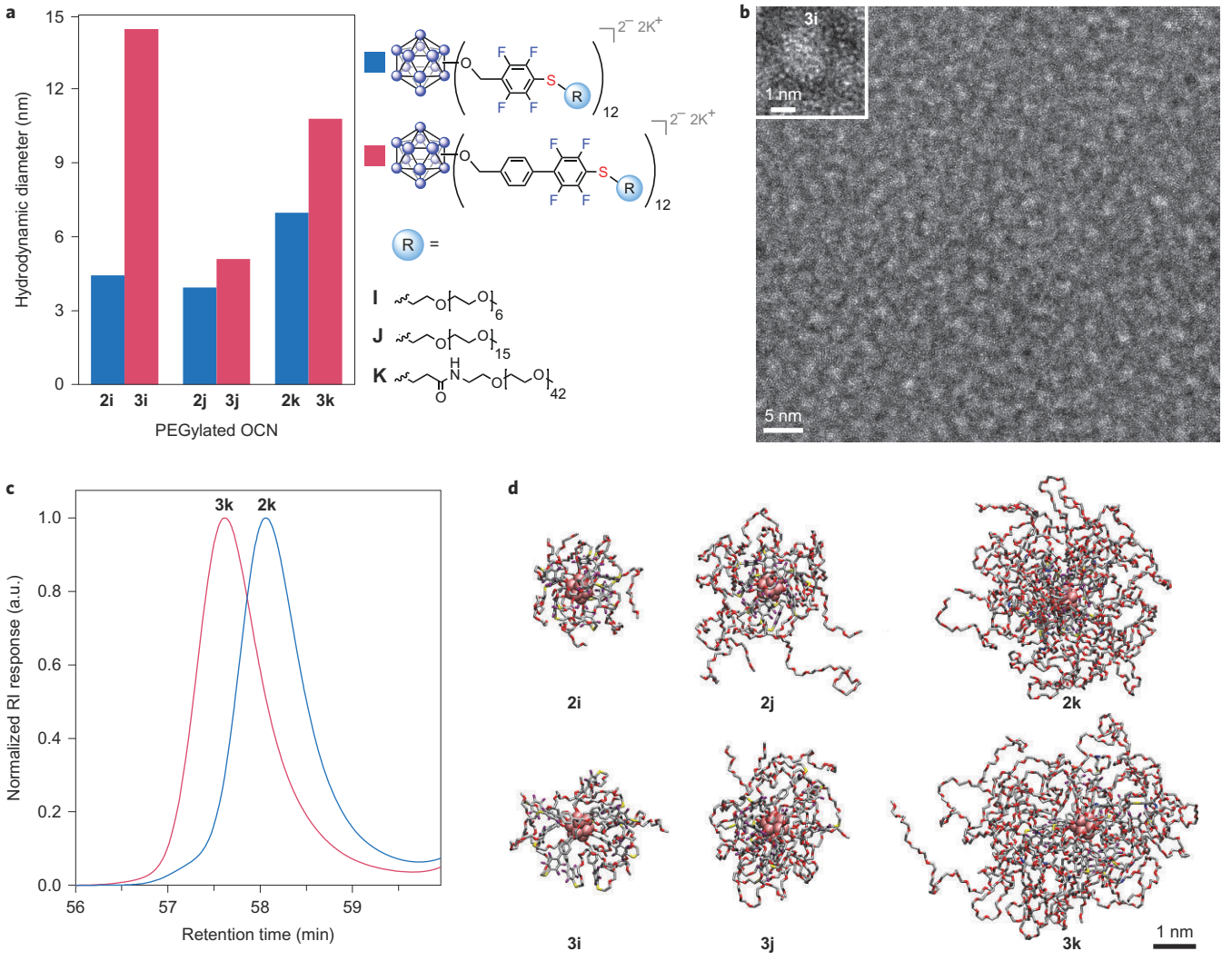


Figure 3 | Characterization of the PEGylated OCNs 2i–2k and 3i–3k. a, Plot of the particle sizes of the PEGylated OCNs **2i**–**2k** and **2i**–**2k** obtained via 2D DOSY ^{1}H NMR experiments. The plot reveals a trend of a gradual increase in the sizes of the OCNs, both as a function of the cluster precursor dimension and of the chain length of the PEG reagent. The size of **3i** is larger than expected, probably because of aggregation. **b**, TEM images of a negatively stained sample of **3i** reveal the presence of nearly monodisperse particles with an average size of 1.9 nm, consistent with the expected size of **3i**. **c**, GPC traces of **2k** and **3k** measured in water further confirm the monodispersity of the samples ($Đ$ = 1.003 ± 0.02 and 1.081 ± 0.007, respectively). **d**, MD-calculated structures of the PEGylated nanomolecules in pure water after 21 ns of simulation indicate a trend in the sizes of the OCNs consistent with that observed through the 2D DOSY experiments (Supplementary Movies 1–6 showcase the dynamics of **2i**–**2k** and **3i**–**3k**). RI, refractive index; a.u., arbitrary units.

yield OCN **2i** (Table 2, entry 1 and Supplementary pages 19, 20 and 91–97). Subsequently, larger mPEG-thiols (M_w = 766 Da and 2,000 Da) were tested and similarly afforded **2j** and **2k**, respectively, in quantitative conversions based on ^{19}F NMR spectroscopy (Table 2, entries 2 and 3 and Supplementary pages 20–23 and 98–110). As expected, PEGylation conferred considerable hydrophilicity to these clusters: **2i**–**2k** are readily soluble in water. Owing to the full covalency of PEGylated OCNs, we hypothesized that these species should be structurally stable under biological conditions. Using **2i** as a model, we conducted stability studies in biologically relevant media (Supplementary pages 204–221). A purified sample of **2i** was exposed to cell-culture media that contained fetal bovine serum for five days at room temperature, and no changes or degradation products were observed by monitoring this sample by ^{19}F and ^{11}B NMR spectroscopy. Similarly, no degradation occurred when this sample was incubated for an additional five days at 37 °C. Importantly, samples of **2i** were dissolved in buffers of various pH (5, 7 and 9) for five days, and these were found to remain structurally intact as well. These results suggest that OCNs retain their structural integrity under the wide range of biologically relevant conditions. We then decided to investigate the stability of the conjugation linkage between the cluster core and the thiol. Given the full covalency of **2i**, we expected that it should not undergo ligand-exchange, a process that commonly occurs with many ligand-capped AuNPs[22]. Significantly, no thiol-exchange occurred when **2i** (0.8 mM) was exposed to 2-mercaptoethanol (20 mM) over a period of 11 days. Similar results were obtained with 2 mM glutathione. Overall, these experiments clearly demonstrate that the OCNs constructed via the S_NAr approach feature superior robustness compared with many AuNP-based assemblies[10,21].

PEGylated OCNs were characterized by a number of techniques to ensure their proposed nearly monodisperse composition (whereas the OCN cores are monodisperse, the PEG chains used in this study feature some compositional variability because of the inherent limitations of PEG oligomer synthesis)[47]. First, we conducted 2D diffusion ordered spectroscopy (2D DOSY) ^{1}H NMR experiments with purified samples of **2i**–**2k** and the more-extended

© 2017 Macmillan Publishers Limited, part of Springer Nature. All rights reserved.

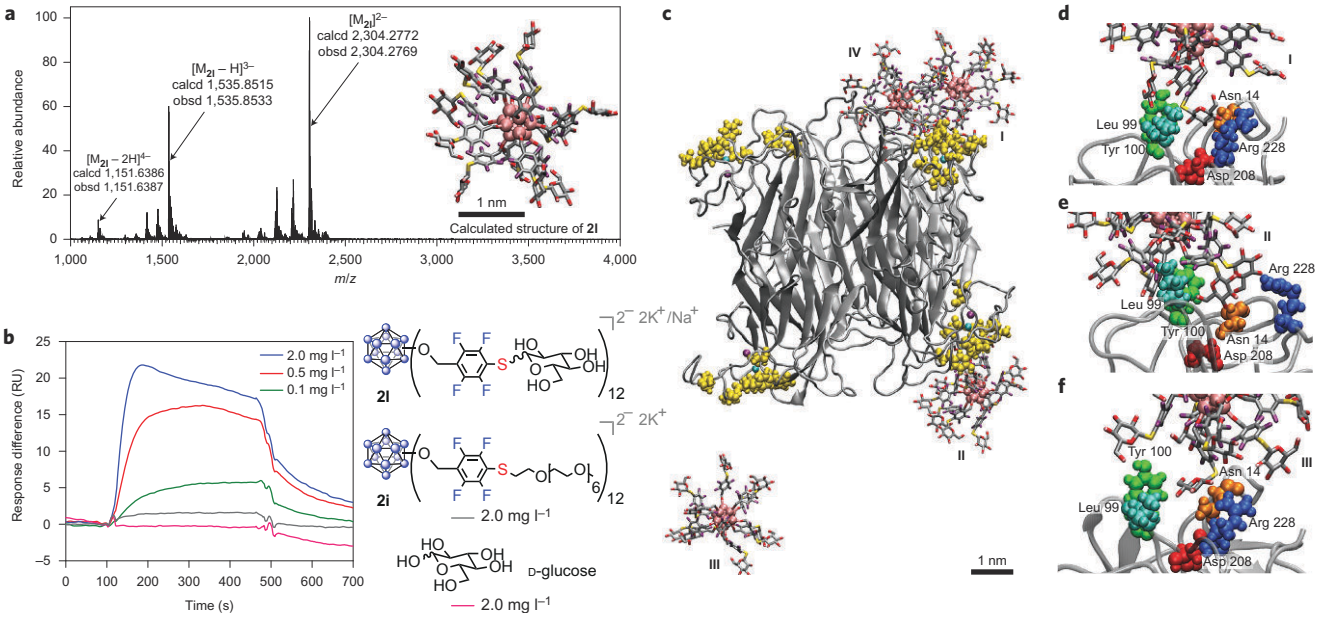


Figure 4 | Multivalent binding of the glycosylated OCN 2l to the lectin ConA. a, ESI-HRMS of **2l** supports its proposed structure and composition (see inset for the MD simulated structure of **2l** in an aqueous environment). **b**, SPR sensorgram indicates that the measured binding response is dependent on the concentration of **2l**. Furthermore, it suggests multivalent binding interactions between **2l** and ConA as well as minimal binding of the PEGylated cluster **2i** and D-glucose controls to ConA. **c**, A snapshot at 20 ns of a MD simulation showcases the interactions between four **2l** particles (I, II, III and IV) and ConA. **d**–**f**, MD-simulation close-up snapshots of three of the **2l** particles (I (**d**), II (**e**) and III (**f**)) binding to ConA at the known monosaccharide-binding residues (coloured and labelled). Supplementary Movie 7 illustrates this simulation and Supplementary Movie 8 illustrates the weakly binding interactions between D-glucose and ConA. Calcd, calculated; obsd, observed.

OCNs **3i**–**3k** (Table 2, entries 5–7 and Supplementary pages 33–36 and 174–190) in D_2O (the 2D DOSY method and plots are given on Supplementary pages 6 and 198–203). Based on the diffusion constants obtained from these 2D DOSY experiments, the respective hydrodynamic diameters were estimated (Fig. 3a). As expected, the results reveal a gradual increase in the sizes of the PEGylated clusters, both as a function of the cluster core size (from **2** to **3**) and the length of the PEG chain used. The size of **3i** measured by 2D DOSY was larger than expected, most probably because of aggregation under the conditions the measurement was performed, which suggests the small number of PEG units in **3i** could not fully stabilize the hydrophobic core against self-aggregation. To determine the size of a single non-aggregated OCN **3i**, we performed additional transmission electron microscopy (TEM) experiments on **3i** (Fig. 3b and Supplementary page 6). The TEM images reveal the presence of nearly monodisperse particles with an average size of 1.9 nm, which is in agreement with the expected value for a non-aggregated single particle. Consistent with these results, gel-permeation chromatography (GPC) traces of **2k** and **3k** in water (Fig. 3c) also reveal nearly monodisperse samples ($Đ = 1.003 \pm 0.02$ and 1.081 ± 0.007, respectively (Supplementary page 6)). Furthermore, we performed molecular dynamics (MD) simulations of species **2i**–**2k** and **3i**–**3k** in water and calculated their hydrodynamic radii and radii of gyration (snapshots after 21 ns are shown in Fig. 3d (Supplementary pages 223–231 and Supplementary Movies 1–6)). The results are in good agreement with the non-aggregated OCN sizes measured by TEM, and moreover exhibit a trend similar to that observed by 2D DOSY. A small discrepancy arises between the sizes estimated based on computational studies/TEM and 2D DOSY and is probably due to some aggregation of the particles under the conditions employed in the 2D DOSY experiments. Overall, our measurements clearly show that using the developed S_NAr assembly strategy, one can rationally prepare robust and nearly monodisperse samples of size-tunable PEGylated OCNs.

After demonstrating the scope of the developed chemistry with various classes of thiols, we next aimed to coat the scaffold clusters with recognition moieties to develop OCNs capable of multivalent binding interactions. In nature, multivalent glycoconjugates, such as glycoproteins and glycolipids, can bind lectins with a relatively high avidity, and thereby bypass the fundamental limitation of weak monosaccharide binding (dissociation constants (K_D) range between millimolar and micromolar)[38,48–52]. We hypothesized that clusters **2** and **3** can serve as rigid, tunable scaffolds for the 3D precise display of saccharides. Using commercially available glucose precursor 1-thio-β-D-glucose tetraacetate, we synthesized the functionalized OCNs **2l** and **3l** featuring 12 appended glucose molecules (Fig. 4a, Table 2, entries 4 and 8 and Supplementary pages 24–25, 36–37, 111–117 and 191–197). We then conducted surface plasmon resonance (SPR) experiments with a Biacore T100 instrument to monitor and quantify binding interactions between the glycosylated OCN **2l** and a model lectin concanavalin A (ConA) at pH 7.4 (Supplementary pages 6 and 7). ConA was covalently attached to the Au-coated sensor chip's dextran layer via conventional amide coupling[53], and binding between ConA and the injected analyte was measured as a change in the refractive index (RI) and expressed in response units (RU). From the binding sensorgrams (Fig. 4b), it is clear that the measured binding response was dependent on the concentration of **2l** in the injected sample. Furthermore, when two controls (**2i** and D-glucose) were injected at the highest mass concentration of **2l** shown (2.0 mg l^{-1}), minimal to no binding was observed. When the binding curves of **2l** were fitted to the Langmuir 1:1 binding model, the K_D value was estimated to be 54 nM, which corresponds to a 6,500-fold increase in affinity when compared with the K_D between ConA and methyl D-glucopyranoside[53]. These results are consistent with the K_D value previously reported by Munoz *et al.* between ConA and a third-generation D-glucose-functionalized glycodendrimer (15.8 nM, 27 saccharides)[53]. This result is significant as it demonstrates that a similar multivalent effect can be achieved by using a rigid OCN

© 2017 Macmillan Publishers Limited, part of Springer Nature. All rights reserved.

scaffold that features significantly fewer (12 versus 27) saccharides. Furthermore, compared with the glycodendrimer used in the work of Munoz and co-workers, which requires eight synthetic steps, glycosylated OCNs can be constructed rapidly (in less than 24 hours) in three steps with an S_NAr conjugation (Huisgen click cycloaddition conjugations on large dendritic assemblies normally take several days for completion)[54]. Lastly, the OCNs generated here are fully covalent and therefore feature enhanced stability properties compared with the species synthesized via a coordination-based self-assembly[55].

We hypothesized that the glycosylated OCN's dramatically enhanced affinity over D-glucose towards ConA can be explained by the cluster glycoside effect[38]. To better understand the mechanistic details of the binding between **2l** and ConA, we performed MD simulations of the interactions between **2l** and ConA (see the snapshots of the simulation in Fig. 4c–f, Supplementary pages 231–237 and Supplementary Movie 7). For comparison, we also simulated interactions between D-glucose and ConA in water (Supplementary pages 231–237 and Supplementary Movie 8). Our calculation results are consistent with the experimental observations—that **2l** exhibits a much higher affinity than the monovalent D-glucose molecule towards ConA's saccharide-binding sites. Furthermore, the higher affinity can be attributed to the multivalent statistical/rebinding effect provided by the densely functionalized surface filled with monosaccharide ligands positioned around the OCN cluster[3,53].

Conclusions

We have developed a new strategy that allows a rapid assembly of fully covalent nanoparticles with atomic precision. Specifically, we demonstrated that the rigid clusters densely decorated with perfluoroaryl-containing functional groups undergo efficient conjugation with a variety of thiols via S_NAr chemistry under very mild conditions at room temperature. Importantly, this chemistry is operationally reminiscent of the chemoselective assembly conditions associated with thiol-capped AuNPs. Furthermore, similarly to thiol-capped AuNPs, these OCNs can be easily tuned in size and surface chemistry by choosing a specific thiol reagent. OCNs exhibit dramatically improved structural stability under a wide range of biologically relevant conditions because of the full covalency of all the bonding interactions that comprise these nanomolecules. Finally, using this assembly strategy we show how one can design and synthesize nanomolecules that feature a 3D densely packed layer of saccharides that can participate in multivalent binding with a natural lectin and lead to a dramatic increase in binding affinity. This work ultimately opens a new avenue to create highly tailored synthetic mimics of ligand-capped AuNPs that feature rigid and fully covalent atomically precise assemblies.

Data availability. The crystallographic data have been deposited at the Cambridge Crystallographic Data Centre (CCDC) as CCDC 1493022 (**2** at 100 K) and 1511361 (**3** at 100 K) and can be obtained free of charge from the CCDC via www.ccdc.cam.ac.uk/getstructures.

Received 26 August 2016; accepted 27 October 2016; published online 19 December 2016

References

1. Mammen, M., Choi, S.-K. & Whitesides, G. M. Polyvalent interactions in biological systems: implications for design and use of multivalent ligands and inhibitors. *Angew. Chem. Int. Ed.* **37,** 2754–2794 (1998).
2. Kiessling, L. L., Gestwicki, J. E. & Strong, L. E. Synthetic multivalent ligands as probes of signal transduction. *Angew. Chem. Int. Ed.* **45,** 2348–2368 (2006).
3. Jones, L. H. Recent advances in the molecular design of synthetic vaccines. *Nat. Chem.* **7,** 952–960 (2015).
4. Elsabahy, M. & Wooley, K. L. Design of polymeric nanoparticles for biomedical delivery applications. *Chem. Soc. Rev.* **41,** 2545–2561 (2012).
5. Rao, J. P. & Geckeler, K. E. Polymer nanoparticles: preparation techniques and size-control parameters. *Prog. Polym. Sci.* **36,** 887–913 (2011).
6. Tomalia, D. A. *et al.* A new class of polymers: starburst-dendritic macromolecules. *Polym. J.* **17,** 117–132 (1985).
7. Hawker, C. J. & Frechet, J. M. J. Preparation of polymers with controlled molecular architecture. A new convergent approach to dendritic macromolecules. *J. Am. Chem. Soc.* **112,** 7638–7647 (1990).
8. Farokhzad, O. C. & Langer, R. Impact of nanotechnology on drug delivery. *ACS Nano* **3,** 16–20 (2009).
9. Peer, D. *et al.* Nanocarriers as an emerging platform for cancer therapy. *Nat. Nanotech.* **2,** 751–760 (2007).
10. Daniel, M.-C. & Astruc, D. Gold nanoparticles: assembly, supramolecular chemistry, quantum-size-related properties, and applications toward biology, catalysis, and nanotechnology. *Chem. Rev.* **104,** 293–346 (2004).
11. Dreaden, E. C., Alkilany, A. M., Huang, X., Murphy, C. J. & El-Sayed, M. A. The golden age: gold nanoparticles for biomedicine. *Chem. Soc. Rev.* **41,** 2740–2779 (2012).
12. Brust, M., Walker, M., Bethell, D., Schiffrin, D. J. & Whyman, R. Synthesis of thiol-derivatised gold nanoparticles in a two-phase liquid–liquid system. *J. Chem. Soc., Chem. Commun.* 801–802 (1994).
13. Giljohann, D. A. *et al.* Oligonucleotide loading determines cellular uptake of DNA-modified gold nanoparticles. *Nano Lett.* **7,** 3818–3821 (2007).
14. Zhao, H. *et al.* Reversible trapping and reaction acceleration within dynamically self-assembling nanoflasks. *Nat. Nanotech.* **11,** 82–88 (2016).
15. Jones, M. R., Seeman, N. C. & Mirkin, C. A. Programmable materials and the nature of the DNA bond. *Science* **347,** 1260901 (2015).
16. Suzuki, K., Sato, S. & Fujita, M. Template synthesis of precisely monodisperse silica nanoparticles within self-assembled organometallic spheres. *Nat. Chem.* **2,** 25–29 (2010).
17. Heindl, C., Peresypkina, E. V., Virovets, A. V., Kremer, W. & Scheer, M. Giant rugby ball $[\{Cp^{Bn}Fe(\eta^5\text{-}P_5)\}_{24}Cu_{96}Br_{96}]$ derived from pentaphosphaferrocene and $CuBr_2$. *J. Am. Chem. Soc.* **137,** 10938–10941 (2015).
18. Ambrogio, M. W., Thomas, C. R., Zhao, Y.-L., Zink, J. I. & Stoddart, J. F. Mechanized silica nanoparticles: a new frontier in theranostic nanomedicine. *Acc. Chem. Res.* **44,** 903–913 (2011).
19. Love, J. C., Estroff, L. A., Kriebel, J. K., Nuzzo, R. G. & Whitesides, G. M. Self-assembled monolayers of thiolates on metals as a form of nanotechnology. *Chem. Rev.* **105,** 1103–1170 (2005).
20. Hostetler, M. J., Green, S. J., Stokes, J. J. & Murray, R. W. Monolayers in three dimensions: synthesis and electrochemistry of ω-functionalized alkanethiolate-stabilized gold cluster compounds. *J. Am. Chem. Soc.* **118,** 4212–4213 (1996).
21. Hostetler, M. J., Templeton, A. C. & Murray, R. W. Dynamics of place-exchange reactions on monolayer-protected gold cluster molecules. *Langmuir* **15,** 3782–3789 (1999).
22. MacLeod, M. J. & Johnson, J. A. PEGylated N-heterocyclic carbene anchors designed to stabilize gold nanoparticles in biologically relevant media. *J. Am. Chem. Soc.* **137,** 7974–7977 (2015).
23. Häkkinen, H. The gold–sulfur interface at the nanoscale. *Nat. Chem.* **4,** 443–455 (2012).
24. Yvon, C. *et al.* Polyoxometalate clusters integrated into peptide chains and as inorganic amino acids: solution- and solid-phase approaches. *Angew. Chem. Int. Ed.* **53,** 3336–3341 (2014).
25. Lachkar, D., Vilona, D., Dumont, E., Lelli, M. & Lacôte, E. Grafting of secondary diolamides onto $[P_2W_{15}V_3O_{62}]^{9-}$ generates hybrid heteropoly acids. *Angew. Chem. Int. Ed.* **55,** 5961–5965 (2016).
26. Gouzerh, P. & Proust, A. Main-group element, organic, and organometallic derivatives of polyoxometalates. *Chem. Rev.* **98,** 77–112 (1998).
27. Müller, A. & Gouzerh, P. From linking of metal–oxide building blocks in a dynamic library to giant clusters with unique properties and towards adaptive chemistry. *Chem. Soc. Rev.* **41,** 7431–7463 (2012).
28. Li, G., Wang, L., Ni, H. & Pittman, C. U. Polyhedral oligomeric silsesquioxane (POSS) polymers and copolymers: a review. *J. Inorg. Organomet. Polym.* **11,** 123–154 (2001).
29. Spokoyny, A. M. New ligand platforms featuring boron-rich clusters as organomimetic substituents. *Pure Appl. Chem.* **85,** 903–919 (2013).
30. Lee, I. S., Long, J. R., Prusiner, S. B. & Safar, J. G. Selective precipitation of prions by polyoxometalate complexes. *J. Am. Chem. Soc.* **127,** 13802–13803 (2005).
31. Pitochelli, A. R. & Hawthorne, M. F. The isolation of the icosahedral $B_{12}H_{12}^{-2}$ ion. *J. Am. Chem. Soc.* **82,** 3228–3229 (1960).
32. Farha, O. K. *et al.* Synthesis of stable dodecaalkoxy derivatives of *hypercloso*-$B_{12}H_{12}$. *J. Am. Chem. Soc.* **127,** 18243–18251 (2005).
33. Jalisatgi, S. S. *et al.* A convenient route to diversely substituted icosahedral closomer nanoscaffolds. *J. Am. Chem. Soc.* **133,** 12382–12385 (2011).
34. Sarma, S. J., Khan, A. A., Goswami, L. N., Jalisatgi, S. S. & Hawthorne, M. F. A trimodal closomer drug-delivery system tailored with tracing and targeting capabilities. *Chem. Eur. J.* **22,** 12715–12723 (2016).
35. Wixtrom, A. I. *et al.* Rapid synthesis of redox-active dodecaborane $B_{12}(OR)_{12}$ clusters under ambient conditions. *Inorg. Chem. Front.* **3,** 711–717 (2016).
36. Messina, M. S. *et al.* Visible-light-induced olefin activation using 3D aromatic boron-rich cluster photooxidants. *J. Am. Chem. Soc.* **138,** 6952–6955 (2016).

© 2017 Macmillan Publishers Limited, part of Springer Nature. All rights reserved.

37. Haynes, W. M. *CRC Handbook of Chemistry and Physics* (CRC/Taylor and Francis, 2016).
38. Lundquist, J. J. & Toone, E. J. The cluster glycoside effect. *Chem. Rev.* **102,** 555–578 (2002).
39. Moore, J. S. & Xu, Z. Synthesis of rigid dendritic macromolecules: enlarging the repeat unit size as a function of generation, permitting growth to continue. *Macromolecules* **24,** 5893–5894 (1991).
40. Birchall, J. M., Green, M., Haszeldine, R. N. & Pitts, A. D. The mechanism of the nucleophilic substitution reactions of polyfluoroarenes. *Chem. Commun. Lond.* 338–339 (1967).
41. Becer, C. R., Hoogenboom, R. & Schubert, U. S. Click chemistry beyond metal-catalyzed cycloaddition. *Angew. Chem. Int. Ed.* **48,** 4900–4908 (2009).
42. Becer, C. R. *et al.* Clicking pentafluorostyrene copolymers: synthesis, nanoprecipitation, and glycosylation. *Macromolecules* **42,** 2387–2394 (2009).
43. Spokoyny, A. M. *et al.* A perfluoroaryl-cysteine S_NAr chemistry approach to unprotected peptide stapling. *J. Am. Chem. Soc.* **135,** 5946–5949 (2013).
44. Zhang, C. *et al.* π-Clamp-mediated cysteine conjugation. *Nat. Chem.* **8,** 120–128 (2016).
45. Hoffman, A. S. The origins and evolution of 'controlled' drug delivery systems. *J. Control. Release* **132,** 153–163 (2008).
46. Alconcel, S. N. S., Baas, A. S. & Maynard, H. D. FDA-approved poly(ethylene glycol)–protein conjugate drugs. *Polym. Chem.* **2,** 1442–1448 (2011).
47. Veronese, F. M. & Pasut, G. PEGylation, successful approach to drug delivery. *Drug Discov. Today* **10,** 1451–1458 (2005).
48. Dam, T. K., Roy, R., Das, S. K., Oscarson, S. & Brewer, C. F. Binding of multivalent carbohydrates to concanavalin A and *Dioclea grandiflora* lectin. Thermodynamic analysis of the 'multivalency effect'. *J. Biol. Chem.* **275,** 14223–14230 (2000).
49. Müller, C., Despras, G. & Lindhorst, T. K. Organizing multivalency in carbohydrate recognition. *Chem. Soc. Rev.* **45,** 3275–3302 (2016).
50. Muñoz, A. *et al.* Synthesis of giant globular multivalent glycofullerenes as potent inhibitors in a model of Ebola virus infection. *Nat. Chem.* **8,** 50–57 (2016).
51. Bhatia, S., Camacho, L. C. & Haag, R. Pathogen inhibition by multivalent ligand architectures. *J. Am. Chem. Soc.* **138,** 8654–8666 (2016).
52. Bernardi, A. *et al.* Multivalent glycoconjugates as anti-pathogenic agents. *Chem. Soc. Rev.* **42,** 4709–4727 (2013).
53. Munoz, E. M., Correa, J., Riguera, R. & Fernandez-Megia, E. Real-time evaluation of binding mechanisms in multivalent interactions: a surface plasmon resonance kinetic approach. *J. Am. Chem. Soc.* **135,** 5966–5969 (2013).
54. Fernandez-Megia, E., Correa, J., Rodríguez-Meizoso, I. & Riguera, R. A click approach to unprotected glycodendrimers. *Macromolecules* **39,** 2113–2120 (2006).
55. Kamiya, N., Tominaga, M., Sato, S. & Fujita, M. Saccharide-coated $M_{12}L_{24}$ molecular spheres that form aggregates by multi-interaction with proteins. *J. Am. Chem. Soc.* **129,** 3816–3817 (2007).

Acknowledgements

A.M.S. acknowledges the University of California, Los Angeles (UCLA) Department of Chemistry and Biochemistry for start-up funds, 3M for a Non-Tenured Faculty Award and the American Chemical Society Petroleum Research Fund (56562-DNI3) for the Doctoral New Investigator Grant. E.A.Q. thanks the US Public Health Service of the National Institutes of Health (NIH) for the Predoctoral Training Fellowship through the UCLA Chemistry-Biology Interface Training Program under the National Research Service Award (T32GM008496). A.S. is funded by the CARE Scholars Programs (NIH grant GM055052). M.S.M. is grateful to the National Science Foundation (NSF) for the Bridge-to-Doctorate and the Predoctoral (GRFP) fellowships. P.K. acknowledges the NSF Division of Materials Research grant 1506886. H.D.M. thanks the NSF (CHE-1507735) for funding. We thank UCLA Molecular Instrumentation Center for mass spectrometry and NMR spectroscopy (NIH grant 1S10OD016387-01, NSF grant CHE-1048804). We also thank the Electron Imaging Center for Nanomachines at the UCLA California NanoSystems Institute for electron microscopy (NIH grant 1S10RR23057) and the UCLA Biochemistry Instrumentation Facility for SPR.

Author contributions

A.M.S. developed the concept and supervised and guided the research. E.A.Q. and A.M.S. designed the experiments. E.A.Q. performed the majority of the experimental work. A.I.W., J.C.A., A.S. and J.Y.W. contributed to the synthesis of **2** and **3**. A.T.R and A.L.R. performed the crystallographic characterization of compound **3**. A.S., E.H.M. and D.M. contributed to the synthesis of **2j** and **3j**. S.C. assisted with optimizing the reaction conditions of **2a–2f**, **2i**, **2l**, **3a–3f**, **3i** and **3l**. A.I.W. and E.H.M. contributed to the purification of the OCNs. D.J. conducted and interpreted the TEM experiments. M.S.M. and H.D.M. assisted with the GPC experiments. P.R., Y.H. and P.K. designed, conducted and interpreted the computational experiments. E.A.Q., A.I.W. and A.M.S. co-wrote the manuscript. All of the authors commented on the manuscript during its preparation.

Additional information

Supplementary information is available in the online version of the paper. Reprints and permissions information is available online at www.nature.com/reprints. Correspondence and requests for materials should be addressed to A.M.S.

Competing financial interests

The authors declare no competing financial interests.

© 2017 Macmillan Publishers Limited, part of Springer Nature. All rights reserved.